Pair plasma relaxation time scales

A. G. Aksenov
Institute for Computer-Aided Design, Russian Academy of Sciences, Vtoraya Brestskaya 19/18, 123056 Moscow, Russia

R. Ruffini and G. V. Vereshchagin
ICRANet, Piazza della Repubblica 10, 65100 Pescara, Italy
and Physics Department, ICRA and University of Rome "Sapienza," Piazzale A. Moro 5, 00185 Rome, Italy

(Received 22 September 2009; revised manuscript received 22 January 2010; published 14 April 2010)

By numerically solving the relativistic Boltzmann equations, we compute the time scale for relaxation to thermal equilibrium for an optically thick electron-positron plasma with baryon loading. We focus on the time scales of electromagnetic interactions. The collisional integrals are obtained directly from the corresponding QED matrix elements. Thermalization time scales are computed for a wide range of values of both the total-energy density (over 10 orders of magnitude) and of the baryonic loading parameter (over 6 orders of magnitude). This also allows us to study such interesting limiting cases as the almost purely electron-positron plasma or electron-proton plasma as well as intermediate cases. These results appear to be important both for laboratory experiments aimed at generating optically thick pair plasmas as well as for astrophysical models in which electron-positron pair plasmas play a relevant role.

DOI: 10.1103/PhysRevE.81.046401 PACS number(s): 52.27.Ep, 31.70.Hq, 52.27.Ny

Current interest in electron-positron plasmas is due to the exciting possibility of generating such plasmas in laboratory facilities already operating or under construction (see, e.g., [1,2]; for a review see [3]). Impressive progress made with ultraintense lasers [4] has led to the creation of positrons at an unprecedented density of 10^{16} cm^{-3} using ultraintense short laser pulses in a region of space with dimensions on the order of the Debye length. However, such densities have not yet reached those necessary for the creation of an optically thick pair plasma [5,6]. Particle pairs are created at the focal point of ultraintense lasers via the Bethe-Heitler conversion of hard x-ray bremsstrahlung photons [1] in the collisionless regime [7]. The approach to an optically thick phase may well be envisaged in the near future.

Electron-positron plasmas are known to be present in compact astrophysical objects, leaving their characteristic imprint in the observed radiation spectra [8]. Optically thick electron-positron plasmas do indeed play a crucial role in the gamma-ray burst (GRB) phenomenon [3,9].

From the theoretical point of view, electron-positron pair plasmas are interesting because of the mass symmetry between the plasma components. This symmetry results in the absence of both acoustic modes and Faraday rotation; waves and instabilities in such plasmas differ significantly from asymmetric electron-ion plasmas (see, e.g., [10]). Besides, theoretical progress in understanding quark-gluon plasma in the high-temperature limit is linked to understanding QED plasma since the results in these two cases differ only by trivial factors containing the QCD degrees of freedom (color and flavor) [2].

Most theoretical considerations so far have assumed that an electron-positron plasma is formed either in thermal equilibrium (common temperature, zero chemical potentials) or in chemical equilibrium (nonzero chemical potentials) (see e.g., [2] and references therein). However, it is necessary to establish the time scale for actually reaching such a configuration. The only way for particles to thermalize, i.e., reach equilibrium distributions (Bose-Einstein or Fermi-Dirac), is via collisions. Collisions become relevant when the mean-free path of the particles becomes smaller than the spatial dimensions of the plasma and so the optical thickness condition is crucial for thermalization to occur.

Thermalization (chemical equilibration) time scales for optically thick plasmas are estimated in the literature by order of magnitude arguments using essentially just the reaction rates of the dominant particle interaction processes (see e.g., [11,12]). They have been computed using various approximations. In particular, electrons have been considered ultrarelativistic and Coulomb logarithm has been replaced by a constant. The accurate determination of such time scales as presented here is instead accomplished by solving the relativistic Boltzmann equations including the collisional integrals representing all possible particle interactions. In this case, the Boltzmann equations become highly nonlinear coupled partial integrodifferential equations which can only be solved numerically.

We developed a relativistic kinetic code treating the plasma as homogeneous and isotropic and have previously determined the thermalization time scales for an electron-positron plasma for selected initial conditions [13]. This approach was generalized to include protons in [14]. We focus only on the electromagnetic interactions, which have a time scale of less than 10^{-9} s for our system, and therefore on the proton and leptonic component of the plasma. The presence of neutrons and their possible equilibrium due to weak interactions will occur only on much longer time scales.

In this paper, we report on the systematic results obtained by exploring the large parameter space characterizing pair plasmas with baryonic loading. The two basic parameters are the total-energy density ρ and the baryonic loading parameter

$$B \equiv \frac{\rho_b}{\rho_{e,\gamma}} \simeq \frac{n_p m_p c^2}{\rho_{e,\gamma}}, \tag{1}$$

where ρ_b and $\rho_{e,\gamma}$ are, respectively, the total-energy densities of baryons and electron-positron-photon plasma, n_p and m_p

TABLE I. Microphysical processes in the pair plasma.

Binary interactions	Radiative and pair-producing variants
Møller and Bhabha $e_1^{\pm}e_2^{\pm}\rightarrow e_1^{\pm\prime}e_2^{\pm\prime}$ $e^{\pm}e^{\mp}\rightarrow e^{\pm\prime}e^{\mp\prime}$	Bremsstrahlung $e_1^{\pm}e_2^{\pm}\leftrightarrow e_1^{\pm\prime}e_2^{\pm\prime}\gamma$ $e^{\pm}e^{\mp}\leftrightarrow e^{\pm\prime}e^{\mp\prime}\gamma$
Single Compton $e^{\pm}\gamma\rightarrow e^{\pm}\gamma'$	Double Compton $e^{\pm}\gamma\leftrightarrow e^{\pm\prime}\gamma'\gamma'$
Pair production and annihilation $\gamma\gamma'\leftrightarrow e^{\pm}e^{\mp}$	Radiative pair production and three-photon annihilation $\gamma\gamma'\leftrightarrow e^{\pm}e^{\mp}\gamma'$ $e^{\pm}e^{\mp}\leftrightarrow\gamma\gamma'\gamma'$ $e^{\pm}\gamma\leftrightarrow e^{\pm\prime}e^{\mp}e^{\pm\prime\prime}$

are the proton number density and proton mass, and c is the speed of light. We choose the following range of plasma parameters

$$10^{23}\leq\rho\leq 10^{33}\ \ \mathrm{erg/cm^3}, \tag{2}$$

$$10^{-3}\leq B\leq 10^{3}, \tag{3}$$

allowing us to also treat the limiting cases of almost pure electron-positron plasma with $B\ll 1$ and almost pure electron-ion plasma with $B\simeq m_p/m_e$, respectively. The temperatures in thermal equilibrium corresponding to Eq. (2) are $0.1\lesssim k_BT\lesssim 10$ MeV.

Given the smallness of the plasma parameter $g=(n_e\lambda_D^3)^{-1}\ll 1$, where λ_D is the Debye length and n_e is the electron number density, it is sufficient to use one-particle distribution functions. In fact, for the pure electron-positron plasma, the inequality $3\times 10^{-3}\leq g\leq 10^{-2}$ holds in the region of the temperatures of interest. In a homogeneous and isotropic plasma, the distribution functions $f(\epsilon,t)$ depend on the energy ϵ of the particle and on the time t. We treat the plasma as nondegenerate, neglecting neutrino channels as well as the creation and annihilation of baryons and the weak interactions [14].

The relativistic Boltzmann equations [15,16] for photons, electrons, positrons, and protons in our case are

$$\frac{1}{c}\frac{\partial f_i}{\partial t}=\sum_q(\eta_i^q-\chi_i^q f_i), \tag{4}$$

where the index i denotes the type of particle and η_i^q, χ_i^q are the emission and the absorption coefficients for the production of the ith particle via the reaction labeled by q. We account for all relevant binary and triple interactions between electrons, positrons, photons, and protons as summarized in Tables I and II.

It has been shown [13] that independent of the functional form of the initial distribution functions $f_i(\epsilon,0)$, plasma evolves to a thermal equilibrium state through the kinetic equilibrium when the distribution functions of all the particles acquire the same form

TABLE II. Microphysical processes in the pair plasma involving protons. For details, see also [3].

Binary interactions (Coulomb scattering)	Radiative and pair-producing variants
$p_1p_2\rightarrow p_1'p_2'$ $pe^{\pm}\rightarrow p'e^{\pm\prime}$	$pe^{\pm}\leftrightarrow p'e^{\pm\prime}\gamma$ $p\gamma\leftrightarrow p'e^{\pm}e^{\mp}$

$$f_i(\varepsilon)=\exp\left(-\frac{\varepsilon-\varphi_i}{\theta_i}\right), \tag{5}$$

where $\varepsilon_i=\epsilon_i/(m_ic^2)$ is the energy of the particles, $\varphi_i\equiv\mu_i/(m_ic^2)$ and $\theta_i\equiv k_BT_i/(m_ic^2)$ are their chemical potentials and temperatures, and k_B is Boltzmann's constant. The unique signature of kinetic equilibrium is the equal temperatures of all the particles and the nonzero chemical potential of the photons. In fact, the same is also true for a pair plasma with proton loading [14]. The approach to complete thermal equilibrium is more complicated in this latter case and depends on the baryon loading. For $B\ll\sqrt{m_p/m_e}$, protons are rare and thermalize via proton-electron (positron) elastic scattering, while in the opposite case $B\gg\sqrt{m_p/m_e}$, proton-proton Coulomb scattering dominates over the proton-electron scattering and brings protons into thermal equilibrium first with themselves. Then, protons thermalize with the pair plasma through triple interactions (for details, see [14]). The two-body time scales involving protons should be compared to the three-body time scales bringing the electron-positron-photon plasma into thermal equilibrium. In fact, we found that for $B\ll 1$, the electron-positron-photon plasma reaches thermal equilibrium at a given temperature, while protons reach thermal equilibrium with themselves at a different temperature; only later the plasma evolves to complete thermal equilibrium with the single temperature on a time scale

$$\tau_{th}\simeq\mathrm{Max}[\tau_{3p},\mathrm{Min}(\tau_{ep},\tau_{pp})], \tag{6}$$

where

$$\tau_{ep}\simeq\frac{m_pc}{\epsilon_e\sigma_Tn_e}, \tag{7}$$

$$\tau_{pp}\simeq\sqrt{\frac{m_p}{m_e}}(\sigma_Tn_pc)^{-1}, \tag{8}$$

$$\tau_{3p}\simeq(\alpha\sigma_Tn_ec)^{-1} \tag{9}$$

are the proton-electron (positron) elastic-scattering time scale, the proton-proton elastic-scattering time scale, and the three-particle interaction time scale, respectively, while σ_T is the Thomson cross section and α is the fine-structure constant. In Eqs. (7)–(9), the energy dependence of the corresponding time scales is neglected.

The chemical relaxation (thermalization) time scale is usually computed as

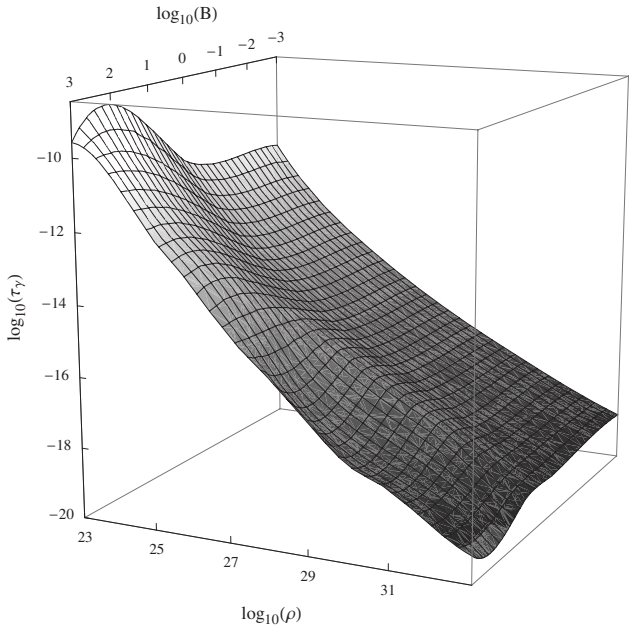

FIG. 1. Thermalization time scale of the electron-positron-photon component of plasma as a function of the total-energy density and the baryonic loading parameter. The energy density is measured in erg/cm^3, time is seconds.

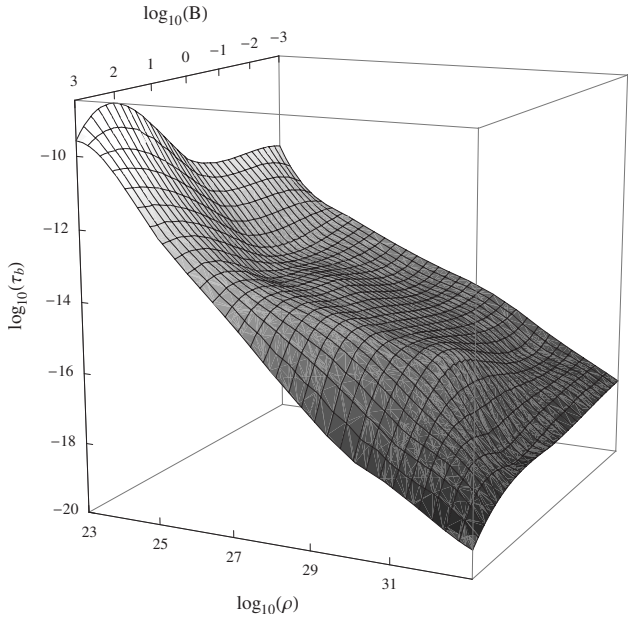

FIG. 2. Final thermalization time scale of a pair plasma with baryonic loading as a function of the total-energy density and the baryonic loading parameter. The energy density is measured in erg/cm^3, time is seconds.

$$\tau_i = \lim_{t\to\infty}\left\{[F_i(t) - F_i(\infty)]\left(\frac{dF_i}{dt}\right)^{-1}\right\}, \tag{10}$$

where $F_i = \exp(\varphi_i/\theta_i)$ is the fugacity of a particle of type i. Instead of F_i, we use one of the quantities θ_i, φ_i, n_i, or ρ_i in this computation.

We solved the Boltzmann equations with parameters (ρ, B) in the range given by Eqs. (2) and (3). In total, 78 models were computed, starting from a nonequilibrium configuration until reaching a steady-state solution on the computational grid with 20 intervals for the particle energy and 16 intervals for the angles (for details, see [14]). For each model, we computed the corresponding time scales for all particles of the ith kind. For practical purposes, instead of Eq. (10), we used the following approximation:

$$\tau_{th} = \frac{1}{t_{fin} - t_{in}}\int_{t_{in}}^{t_{fin}} [\theta(t) - \theta(t_{\max})]\left(\frac{d\theta}{dt}\right)^{-1} dt, \tag{11}$$

with $t_{in} < t_{fin} < t_{\max}$, where $t_{\max}$ is the moment of time where the steady solution is reached and t_{in} and t_{fin} are the boundaries of the time interval over which the averaging is performed (for details, see [17]). The thermalization time scale of the electron-positron-photon component is shown in Fig. 1 as a function of the total-energy density of the plasma and the baryonic loading parameter. The time scales of electrons, positrons, and photons coincide. The final thermalization time scale of pair plasma with baryonic loading is shown in Fig. 2. Its dependence on either variable cannot be fit by a simple power law, although it decreases monotonically with increasing total-energy density, while it is not even a monotonic function of the baryonic loading parameter.

In Fig. 3, the final thermalization time scale is shown for all the models we computed, along with the "error bars" which mark one standard deviation of the time scale (11) away from the average value τ_{th} in the averaging interval $t_{in} \le t \le t_{fin}$. The largest source of error comes from the small values of the time derivative in Eq. (11), although errors are typically below a few percent.

In Fig. 4, we compare for $B=1$ the actual value of the thermalization time scale of the electron-positron-photon component to the value estimated from Eq. (9). Both values clearly differ significantly. Actually, the systematic underestimation by more than 1 order of magnitude which occurs for $B \le 1$ disappears for larger baryonic loading.

In Fig. 5, we present the computed values of the final thermalization time scale of the pair plasma with baryonic

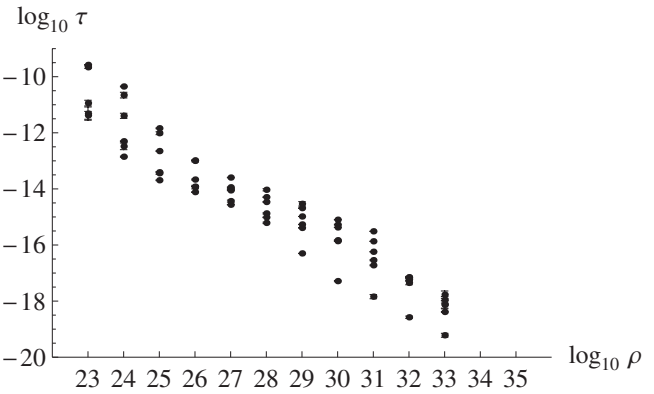

FIG. 3. Final thermalization time scale of pair plasma with baryonic loading as a function of the total-energy density for selected values of the baryonic loading parameter $B = (10^{-3}, 10^{-1.5}, 1, 10, 10^2, 10^3)$. The energy density is measured in erg/cm^3, time is seconds. Error bars correspond to one standard deviation of the time scale (11) away from the average value τ_{th} over the interval $t_{in} \le t \le t_{fin}$.

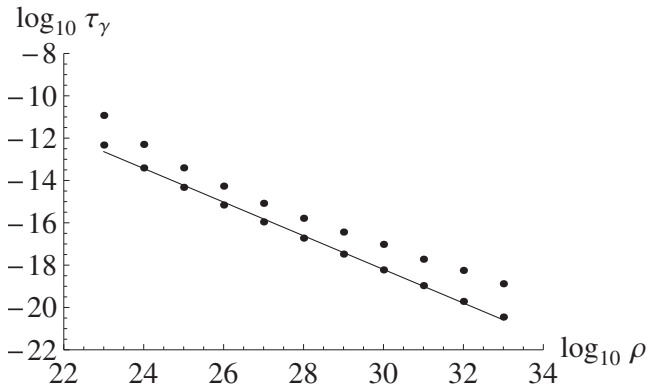

FIG. 4. Thermalization time scale of the electron-positron-photon component of the plasma as a function of the total-energy density (points) compared to the τ_{3p} time scale (joined points) computed using Eq. (9) for $B=1$. The energy density is measured in erg/cm^3, time is seconds.

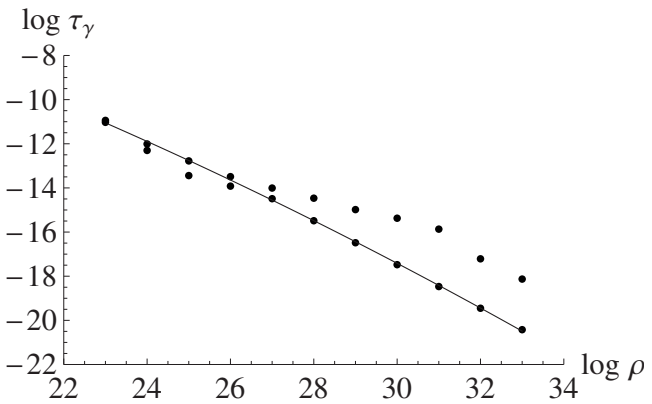

FIG. 5. Final thermalization time scale of a pair plasma with baryonic loading as a function of the total-energy density (points), compared to the τ_{th} time scale (joined points) computed using Eq. (6) for $B=1$. The energy density is measured in erg/cm^3, time is seconds.

loading together with the value estimated from Eq. (6), again for $B=1$. Unlike the previous case, the final thermalization time scale is a more complex function of the total-energy density. Interestingly, less significant deviations from the value (6) occur at the extremes of the interval (3).

In this paper, we have computed the time scale of thermalization for an electron-positron plasma with proton loading over wide ranges of both the total-energy density (10 orders of magnitude) and baryonic loading parameter (6 orders of magnitude), allowing the treatment of the limiting cases of almost pure electron-positron plasma, almost pure electron-ion plasma, as well as intermediate cases. The final result is presented in Figs. 1 and 2. The relaxation to thermal equilibrium for the total-energy density (2) always occurs on a time scale less than 10^{-9} s. It is interesting that the electron-positron-photon component and/or proton component can thermalize earlier than the time at which complete thermal equilibrium is reached. The relevant time scales are given and compared to the order-of-magnitude estimates. Unlike previous work, there are no simplifying assumptions in our method since collisional integrals in the Boltzmann equations are computed directly from the corresponding QED matrix elements, e.g., from the first principles.

These results may be of relevance for the ongoing and future laboratory experiments aimed at creating electron-positron plasmas. Current optical lasers producing pulses during $\sim 10^{-15}$ s carrying energy $\sim 10^2$ J$=10^9$ erg are capable to produce positrons with the number density 10^{16} cm^{-3} [4]. There are claims that densities of the order of 10^{22} cm^{-3} are reachable [18]. These densities today are yet far from 10^{28} cm^{-3} required for the plasma with the size $r_0 \simeq \mu$m to be optically thick [5]. Notice that the expansion time scale of such plasma will be $r_0/c \sim 10^{-14}$ s, while the time scale to establish kinetic equilibrium for the number density considered is of the same order of magnitude. These arguments show that theoretical results obtained assuming thermal or kinetic equilibrium, such as in [2], cannot be applied to pair plasma, generated by ultraintense lasers.

However, results presented in this paper are important for understanding astrophysical systems observed today in which optically thick electron-positron plasmas are present. As specific example, we recall that electron-positron pairs play the crucial rule in the dynamics of GRB sources. Considering typical energies and initial radii for GRB progenitors [19]

$$10^{48}\ \text{erg} < E_0 < 10^{54}\ \text{erg}, \quad 10^7\ \text{cm} < R_0 < 10^8\ \text{cm}, \tag{12}$$

we estimate the range for the energy density in GRB sources

$$10^{23}\frac{\text{erg}}{\text{cm}^3} < \rho < 10^{32}\frac{\text{erg}}{\text{cm}^3}, \tag{13}$$

which coincides with Eq. (2). As for the baryonic loading of GRBs, it is typically in the lower range of Eq. (2), namely [9],

$$10^{-3} < B < 10^{-2}. \tag{14}$$

Such high-energy density leads to large number density of electron-positron pairs in the source of GRB of the order of

$$10^{30}\ \text{cm}^{-3} < n < 10^{37}\ \text{cm}^{-3}, \tag{15}$$

making it opaque to photons with huge optical depth of the order of

$$10^{13} < \tau < 10^{18}. \tag{16}$$

In fact, the radiative pressure of optically thick electron-positron plasma in these systems is responsible for the effect of accelerated expansion [9,20–22] leading to unprecedented Lorentz factors attained $\Gamma \simeq B^{-1}$ up to 10^3 (see, e.g., [23,24]). The role of the baryon admixture in electron-positron plasma in GRBs is to transfer internal energy of pairs and photons into kinetic energy of the bulk motion thus giving origin to afterglows of GRBs [9,19]. Notice that in GRBs the time scales of thermalization are much shorter than the dynamical time scales $R_0/c \sim 10^{-3}$ s, which implies that expanding electron-positron plasma even in the presence of baryons is in thermal equilibrium during the accelerating optically thick phase [25].

After completion of this work, we learned about the publication of [26] where work similar to ours has been per-

formed. Between this paper and our work, conceptual differences should be noted which concern the attribution of thermalization to two-body Møller and Bhabha scattering, while we have pointed out explicitly that three-body interactions play an essential role. The thermalization time scales obtained by us have been computed with reference to these three-body interactions.

We thank both anonymous referees for their comments which allowed the remarkable improvement of the paper.

[1] J. Myatt, J. A. Delettrez, A. V. Maximov, D. D. Meyerhofer, R. W. Short, C. Stoeckl, and M. Storm, Phys. Rev. E **79**, 066409 (2009).
[2] M. H. Thoma, Rev. Mod. Phys. **81**, 959 (2009).
[3] R. Ruffini, G. Vereshchagin, and S.-S. Xue, Phys. Rep. **487**, 1 (2010).
[4] H. Chen, S. C. Wilks, J. D. Bonlie, E. P. Liang, J. Myatt, D. F. Price, D. D. Meyerhofer, and P. Beiersdorfer, Phys. Rev. Lett. **102**, 105001 (2009).
[5] J. I. Katz, Astrophys. J., Suppl. Ser. **127**, 371 (2000).
[6] M. G. Mustafa and B. Kämpfer, Phys. Rev. A **79**, 020103(R) (2009).
[7] S. C. Wilks, W. L. Kruer, M. Tabak, and A. B. Langdon, Phys. Rev. Lett. **69**, 1383 (1992).
[8] E. Churazov, R. Sunyaev, S. Sazonov, M. Revnivtsev, and D. Varshalovich, Mon. Not. R. Astron. Soc. **357**, 1377 (2005).
[9] R. Ruffini *et al.*, in *American Institute of Physics Conference Series*, edited by M. Novello and S. Perez, AIP Conference Series Vol. 1132 (AIP, New York, 2009), pp. 199–266.
[10] G. P. Zank and R. G. Greaves, Phys. Rev. E **51**, 6079 (1995).
[11] R. J. Gould, Phys. Fluids **24**, 102 (1981).
[12] S. Stepney, Mon. Not. R. Astron. Soc. **202**, 467 (1983).
[13] A. G. Aksenov, R. Ruffini, and G. V. Vereshchagin, Phys. Rev. Lett. **99**, 125003 (2007).
[14] A. G. Aksenov, R. Ruffini, and G. V. Vereshchagin, Phys. Rev. D **79**, 043008 (2009).
[15] S. Belyaev and G. Budker, Dokl. Akad. Nauk SSSR **107**, 807 (1956).
[16] D. Mihalas and B. W. Mihalas, *Foundations of Radiation Hydrodynamics* (Oxford University Press, New York, 1984).
[17] A. G. Aksenov, R. Ruffini, and G. V. Vereshchagin, AIP Conf. Proc. **1205**, 11 (2010).
[18] B. Shen and J. Meyer-ter-Vehn, Phys. Rev. E **65**, 016405 (2001).
[19] T. Piran, Phys. Rep. **314**, 575 (1999).
[20] R. Ruffini, J. D. Salmonson, J. R. Wilson, and S.-S. Xue, Astron. Astrophys. **350**, 334 (1999).
[21] R. Ruffini, J. D. Salmonson, J. R. Wilson, and S.-S. Xue, Astron. Astrophys. **359**, 855 (2000).
[22] C. L. Bianco, R. Ruffini, G. Vereshchagin, and S.-S. Xue, J. Korean Phys. Soc. **49**, 722 (2006).
[23] A. A. Abdo *et al.*, Science **323**, 1688 (2009).
[24] L. Izzo *et al.*, Proceedings of the First Galileo—Xu Guangqi Meeting, Shanghai, China, October 2009 (unpublished).
[25] A. G. Aksenov, C. L. Bianco, R. Ruffini, and G. V. Vereshchagin, AIP Conf. Proc. **1000**, 309 (2008).
[26] I. Kuznetsova, D. Habs, and J. Rafelski, Phys. Rev. D **81**, 053007 (2010).